HOKKAIDO UNIVERSITY

Title	Reaction Mechanism of FePS3 Electrodes in All-Solid-State Lithium Secondary Batteries Using Sulfide-Based Solid Electrolytes
Author(s)	Fujii, Yuta; Miura, Akira; Rosero-Navarro, Nataly Carolina et al.
Citation	Journal of The Electrochemical Society, 165(13), A2948-A2954 https://doi.org/10.1149/2.0191813jes
Issue Date	2018-09-15
Doc URL	https://hdl.handle.net/2115/76122
Rights	© The Electrochemical Society, Inc. 2018. All rights reserved. Except as provided under U.S. copyright law, this work may not be reproduced, resold, distributed, or modified without the express permission of The Electrochemical Society (ECS). The archival version of this work was published in J. Electrochem. Soc. 2018 volume 165, issue 13, A2948-A2954.
Type	journal article
File Information	HUSCUP J. Electrochem. Soc. A2948-A2954 Accept manuscript.pdf

Hokkaido University Collection of Scholarly and Academic Papers

Hokkaido University Collection of Scholarly and Academic Papers : HUSCAP

Reaction mechanism of $FePS_3$ electrodes in all-solid-state lithium secondary batteries using sulfide-based solid electrolytes

Yuta Fujii[a], Akira Miura[b*], Nataly Carolina Rosero-Navarro[b], Yoshikazu Mizuguchi[c], Chikako Moriyoshi[d], Yoshihiro Kuroiwa[d], Mikio Higuchi[b], Kiyoharu Tadanaga[b]

[a]Graduate School of Chemical Sciences and Engineering, Hokkaido University, Sapporo 060-8628, Japan

[b]Faculty of Engineering, Hokkaido University, Sapporo 060-8628, Japan

[c]Graduate School of Science and Engineering, Tokyo Metropolitan University, Hachioji 192-0397, Japan

[d]Department of Physical Science, Hiroshima University, Higashihiroshima 739-8526, Japan

[*]Corresponding Author

E-mail address: amiura@eng.hokudai.ac.jp (A. Miura)

Abstract

In this study, we investigated the reaction mechanism of the $FePS_3$ electrode in all-solid-state lithium secondary batteries that utilized sulfide-based solid electrolytes by X-ray diffraction patterns, X-ray absorption spectra, Raman spectra, and density-functional theory (DFT) calculation. In discharge-charge measurements, the reversible discharge-charge reaction ($FePS_3 + xLi^+ + xe^- \rightleftarrows Li_xFePS_3$, $0 \leq x \leq 1.5$) was confirmed. With this reaction, Li^+-inserted $FePS_3$ with low crystallinity was formed with the reduction of iron during the discharge cycle, and crystalline $FePS_3$ appeared along with the oxidation of iron during the charge cycle. Raman spectra showed that $P_2S_6^{4-}$ units were not destroyed during this discharge-charge cycle. In the second cycle, the discharge voltage of the batteries that used $FePS_3$ increased relative to that at the first cycle. The reversible change in chemical states of iron and sulfur was confirmed by X-ray absorption. The first-principle calculation explained the experimental results of the change of crystalline phase and the increase in the discharge voltage. Further, the calculation results indicated that not only iron but also sulfur was oxidized and reduced from the first charge cycle onwards.

Introduction

Lithium secondary batteries with high operating voltage and long life cycles have been used as power sources for portable electronic devices such as mobile phones and laptops.[1,2] These batteries are expected to be utilized as large-scale energy-storage systems (ESSs); therefore, the development of batteries with high safety and high energy density is required.

In lithium-ion secondary batteries, lithium transition-metal oxides (e.g., $LiCoO_2$,[3,4] $LiNiO_2$,[5] $LiMn_2O_4$,[6] and $LiCo_{1/3}Ni_{1/3}Mn_{1/3}O_2$[7]) and lithium iron phosphate ($LiFePO_4$)[8] with actual capacities of 100–160 mAh g^{-1} have been used as cathode active materials. These capacities from the redox reaction of the transition metal need to be increased to develop batteries with high energy density. Recently, lithium-excess transition-metal oxides have been considered for use as high-capacity cathode active materials[9–13] because these active materials have capacities of more than 200 mAh g^{-1} based on the redox reactions of the transition metal and oxygen. Moreover, transition-metal sulfides (e.g., FeS_2[14] and MoS_3[15]) have been considered as cathode active materials with high capacity based on the redox reaction of transition metals and sulfur. Hence, not only the redox reaction of the transition metal but also that of the anion is important for increasing the

capacity of active materials.

Recently, all-solid-state lithium secondary batteries that use nonflammable inorganic solid electrolytes instead of flammable organic-liquid electrolytes have been investigated[16,17] because of their high safety and potential for high energy density. To improve the electrochemical performance of all-solid-state batteries, the development of solid electrolytes with high lithium-ion conductivity and the formation of a suitable low-resistance interface between electrodes and electrolytes are key points. Sulfide-based solid electrolytes have been reported to show high lithium-ion conductivities that are comparable to those of organic-liquid electrolytes.[18–21] There are many reports involving all-solid-state batteries that utilize Li_2S_5-P_2S_5 solid electrolytes.[22–26] In order to form the electrode-electrolyte interfaces with low resistance, composite electrodes are used because there is a large contact area between electrodes and electrolytes, as well as sufficient paths for lithium ions and electron conduction. Composite electrodes are prepared by mixing an active material with a solid electrolyte and a conductive additive.

Transition-metal sulfides (e.g., FeS,[27] FeS_2,[28] C-FeS_2-S,[29] TiS_2,[30] amorphous TiS_3, [31] Li_2TiS_3,[32] amorphous TiS_4,[33] and MoS_3[34]) have been investigated as active materials in all-solid-state lithium secondary batteries using sulfide-based solid electrolytes. There are

two types of active materials: one utilizes the redox reaction of only transition metals and the other utilizes the reaction of both sulfur and transition metals.[14,15,35] Notably, the transition-metal sulfides with high capacity associated with the redox reaction of sulfur and transition metal should be used to develop batteries with high energy density. Transition-metal sulfide active materials have two advantages in all-solid-state batteries using sulfide-based solid electrolytes. First, using transition-metal sulfides, all-solid-state batteries are expected to show better cycling performance than batteries that use liquid electrolytes for the following reasons. Some transition-metal sulfides form polysulfides during the discharge process.[28,36] These polysulfides dissolve in liquid electrolytes. Hence, in batteries that use liquid electrolytes, the loss of active materials owing to the dissolution causes capacity degradation. However, in all-solid-state batteries that do not use liquid electrolytes, the problem of the dissolution can be solved. Thus, all-solid-state batteries that use transition-metal sulfides are expected to show good cycling performance. Secondly, suitable electrode-electrolyte interfaces with low resistance are expected to be maintained in all-solid-state batteries that use transition-metal sulfides and sulfide-based solid electrolytes during the charge process. Unfortunately, in all-solid-state batteries that use high-voltage oxide-based cathode active materials and sulfide-based solid electrolytes, interfacial layers with high resistance can be formed in electrode-electrolyte interfaces.[37]

However, the interfacial layers with high resistance are not expected to be formed in all-solid-state batteries using transition-metal sulfides and sulfide-based solid electrolytes because of the similarities in their composition.

We have previously investigated $FePS_3$ as active materials with layered structures in all-solid-state batteries that use sulfide-based solid electrolytes.[38] $FePS_3$, which contains abundant iron in the earth's crust, has a moderate electronic conductivity (~10^{-5} S cm^{-1}),[39] and is expected to show high lithium-ion diffusion because of the layer structure. Because sufficient paths of lithium ions and of electron conduction should be formed in electrodes, $FePS_3$ has potential as active materials in all-solid-state batteries. In a previous report, $FePS_3$ was intercalated with 1.5 mol of Li^+ per 1.0 mol of Fe in batteries that use liquid electrolytes,[40] as shown in reaction (1).

$$FePS_3 + 1.5\ Li^+ + 1.5\ e^- \rightleftarrows Li_{1.5}FePS_3 \qquad (1)$$

In this reversible intercalation reaction, the theoretical capacity is 220 mAh g^{-1}. Moreover, $FePS_3$ can react with 9.0 mol of Li^+ per Fe in batteries that use organic-liquid electrolytes,[40] as shown in reactions (2) and (3).

$$Li_{1.5}FePS_3 + 4.5\ Li^+ + 4.5\ e^- \rightarrow 3\ Li_2S + Fe + P \qquad (2)$$

$$P + 3\ Li^+ + 3\ e^- \rightarrow Li_3P \qquad (3)$$

In this irreversible conversion reaction, the theoretical capacity is 1318 mAh g^{-1}. We reported that all-solid-state lithium secondary batteries that use $FePS_3$ and sulfide-based

solid electrolytes showed discharge-charge behavior.[38] However, the reaction mechanism of $FePS_3$ is unclear in all-solid-state lithium secondary batteries. With respect to the discharge-charge behavior, the discharge voltage of the batteries increased from the second cycle onwards. The reason for the increase in the discharge voltage has not been well investigated, and a study to clarify the reaction mechanism of $FePS_3$ may be useful to gain an understanding of layered transition-metal sulfide active materials in all-solid-state batteries.

In this study, we investigated the reaction mechanism of $FePS_3$ in all-solid-state lithium secondary batteries using sulfide-based solid electrolytes. In discharge-charge measurements, the reversible discharge-charge reaction ($FePS_3 + xLi^+ + xe^- \rightleftarrows Li_xFePS_3$, $0 \leq x \leq 1.5$) was observed. The changes in chemical states of iron and sulfur during discharge-charge cycles were confirmed by Fe and S K-edge absorption near-edge structure (XANES) spectra. The results of the first-principle calculations indicated that not only iron but also sulfur was oxidized and reduced from the first charge cycle onwards.

Experimental

An $FePS_3$ was synthesized by heating elemental iron powder (Wako Chemical, 99.9%), red phosphorus (Kanto Chemical, 98.0%), and sulfur (Kanto Chemical, 99.5%) in an

evacuated quartz tube.[40] Iron powder, red phosphorus, and sulfur were mixed at a molar ratio of 1.00:1.15:3.45 using an agate mortar. The mixture was sealed in an evacuated quartz tube and heated at 998 K for 24 h. After the reaction, the obtained sample was heated at 598 K for 20 min under vacuum to remove excess red phosphorus and sulfur relative to their stoichiometric amount. After grinding the product using an agate mortar, the ground powder was passed through a 100-μm sieve to remove particles larger than 100 μm.

All-solid-state batteries of Li-In/$75Li_2S{\cdot}25P_2S_5$ (mol%) glass/$FePS_3$ were fabricated according to a previous report.[16] All of the processes mentioned below were performed under a dry Ar atmosphere. The $75Li_2S{\cdot}25P_2S_5$ glass-solid electrolyte with an ambient temperature conductivity of around 10^{-4} S cm^{-1} was prepared by the mechanical milling of reagent-grade Li_2S (Mitsuwa Chemical, 99.9%) and P_2S_5 (Aldrich, 99%) powders.[41] A composite electrode was prepared as a working electrode by mixing $FePS_3$, the $75Li_2S{\cdot}25P_2S_5$ glass, and vapor-grown carbon fibers (VGCF, Showa Denko) with a weight ratio of 69:29:2. The composite electrode (10 mg) or only $FePS_3$ (10 mg) and the $75Li_2S{\cdot}25P_2S_5$ glass-solid electrolyte (120 mg) were placed into a polycarbonate tube (ϕ = 10 mm), and pressed together under 360 MPa. Then, a Li-In alloy foil used as a counter electrode was pressed under 120 MPa. After pressing, the obtained pellet was

sandwiched by two stainless-steel disks as current collectors. The batteries were discharged and charged under a constant current density of 0.13 mA cm^{-2} at room temperature (typically 293–298 K), using a discharge-charge measuring device (Scribner Associates, 580 battery-type system). In discharge-charge measurements, we investigated the effect of the amount of inserted Li^+ in $FePS_3$ on the discharge-charge behavior. In order to investigate the change in the crystalline structures of $FePS_3$ during discharge-charge cycles, ex-situ X-ray diffraction (XRD) patterns of the $FePS_3$ composite electrodes before and after the discharge/charge were recorded using synchrotron X-ray sources at the SPring-8 BL02B2 beam line (proposal No. 2016B1078). Raman spectra of the $FePS_3$ composite electrodes before and after discharge/charge were measured using a Raman spectrometer (XploRA, Horiba) with a green laser (Wavelength: 532 nm) to investigate the change in the $P_2S_6^{4-}$ units in $FePS_3$ during discharge-charge cycles. In the XRD and Raman measurements, evacuated capillary glass tubes were used to seal the samples. The absorption near-edge structure (XANES) spectra were measured before and after discharge/charge. The spectra of Fe K-edge were measured using the $FePS_3$ composite electrodes and those of S K-edge were measured using $FePS_3$ electrodes without solid electrolytes. XANES spectra were measured at the BL5S1 (proposal No. 201606008) and BL6N1 (proposal No. 201802083) of the Aichi Synchrotron Center, Aichi Science &

Technology Foundation. Redox reactions of iron and sulfur in $FePS_3$ during the discharge-charge process were investigated. Based on the results obtained for the above-mentioned measurements, first-principle calculations were performed using the Vienna Ab initio Simulation Package (VASP). The equilibrium voltage of the reaction of $FePS_3$ with Li^+ and density of states (DOSs) of $FePS_3$ and Li^+-inserted $FePS_3$ were calculated using the optimized structure models of $FePS_3$ and Li^+-inserted $FePS_3$. Structure models of $FePS_3$ before and after discharge/charge were illustrated using VESTA.

3. Results and Discussion

Figure 1 shows (a) first and (b) second discharge-charge curves of all-solid-state batteries of Li-In/$75Li_2S{\cdot}25P_2S_5$/$FePS_3$ at 0.13 mA cm^{-2} at room temperature. Based on the reported reaction of $FePS_3$ with 0–1.5 mol Li^+,[40] 0.5-mol (solid lines), 1.0-mol (dashed lines), and 1.5-mol (dashed-dotted lines) Li^+ were first inserted into $FePS_3$ in the first discharge cycle. Then, the discharge-charge cycles were repeated between 0.91–2.2 V vs. Li-In. The batteries showed similar discharge-charge behaviors, indicating that the same discharge-charge reaction occurred with a range below 1.5-mol Li^+ per $FePS_3$. Thus, we investigated further the reaction mechanism with the insertion of 1.5 mol of Li^+. To discuss the overvoltage of the batteries, the open-circuit voltage (OCVs) were measured

at several points shown in Figure 1 (a) (A)-(D). The OCVs (A) before discharge and charge, (B) after the first discharge, (C) at 1.5 V vs. Li-In during charge, and (D) after the first charge were 1.28 V, 0.92 V, 1.48 V, 2.14 V vs. Li-In, respectively. These results suggest a small overvoltage of the batteries.

Figure 2 shows XRD patterns of the $FePS_3$ composite electrode (a) before discharge and charge, (b) after the first discharge, (c) first charge, and (d) second discharge cycles. Before the discharge and charge, the diffraction peaks due to $FePS_3$ were observed. After the first discharge, the intensity of the peaks due to $FePS_3$ became significantly weak, and only broad peaks were observed. After the first charge, strong peaks due to $FePS_3$ were observed. After the subsequent second discharge, the intensity of the peaks due to $FePS_3$ again became weak. The change in intensity of the peaks owing to $FePS_3$ reveals that Li^+-inserted $FePS_3$ with low crystallinity is formed after the discharge and crystalline $FePS_3$ is formed after the charge. Although the peak position at 6.42 Å, which corresponded to 001 diffraction, was unchanged (a) before discharge and charge and (c) after the first charge, the peak had a tail toward the higher angle after the first charge. This tail can be explained by the insertion of Li^+ into the interlayer of $FePS_3$. Thus, Li^+ would be (at least partially) inserted and extracted into and from the interlayer of $FePS_3$ during the discharge-charge process.

Figure 3 presents Raman spectra of the $FePS_3$ composite electrode (a) before discharge and charge, (b) after the first discharge, (c) first charge, and (d) second discharge cycles. The Raman bands that are attributed to $P_2S_6^{4-}$ were observed before and after the discharge/charge.[42] This indicates that $P_2S_6^{4-}$ units in $FePS_3$ are not destroyed during discharge-charge cycles, even in the low-crystallinity phase detected by XRD. The peak position shifted to a higher wavenumber after the second discharge, indicating that the symmetry of $P_2S_6^{4-}$ changes after the second discharge. The peak width increased after the discharge. This indicates a local disordering in Li^+-inserted $FePS_3$ after discharge. This result is in good agreement with that obtained for the formation of a low-crystallinity phase during discharge cycles in the XRD patterns.

Fe K-edge XANES spectra of the $FePS_3$ composite electrode (a) before discharge and charge, (b) after the first discharge, (c) first charge, and (d) second discharge cycles are shown in Figure 4. For comparison, the spectrum of (e) Fe metal that is used as a reference is also shown. The oxidation state of iron in $FePS_3$ has reported to be 2+.[40] After the first and second discharge, the spectrum of the $FePS_3$ electrode shifted to the low energy side, indicating that the valence of iron in $FePS_3$ decreased during the discharge process. These spectra were different from that of Fe metal, indicating the valence of iron is above zero. In contrast, the spectrum of the $FePS_3$ electrode shifted to the high-energy side after the

first charge although this is not the same as pristine spectra. This indicates that the valence of iron in $FePS_3$ increases but below 2+ during the charge process. These results reveal that iron is reduced and oxidized during discharge-charge cycles. Although the quantitative analysis of Fe valence is difficult to be determined, the spectrum change between discharge and charge is smaller if one assume the oxidation and reduction between 0.5+ and 2+. This indicates that sulfur can also be oxidized at the first charge cycle and reduced at the second discharge cycle. To investigate the redox reaction of sulfur before and after discharge and charge, S K-edge XANES spectra of the $FePS_3$ electrode without solid electrolytes were measured (Figure 5). In sulfur K-edge spectra of the $FePS_3$ electrolytes, a peak at 2471.2 eV was observed before discharge and charge. After the first discharge, the peak intensity was decreased, and the profile shape changed slightly. This profile was different to that of elemental sulfur.[43] After the first charge, the peak intensity at 2471.2 eV was increased, and the profile shape was similar to that before discharge and charge. After the second discharge, the peak intensity was decreased again. The profile shape was similar to that after the first discharge. The similar change of the peak intensity before and after discharge and charge was confirmed in S K-edge XANES spectra of the Li_3PS_4-carbon during charge-discharge cycles.[44] These results suggest that the chemical state of sulfur in $FePS_3$ changes reversibly during discharge-charge cycles

although there was no evidence of the sulfur redox.

The results obtained so far reveal that Li^+ can be inserted and extracted into and from the interlayer of $FePS_3$ during the discharge-charge cycle with a range below 1.5-mol Li^+ per 1.0 mol of $FePS_3$. While Li^+-inserted $FePS_3$ with low crystallinity was formed during the discharge cycle, crystalline $FePS_3$ was formed during the charge cycle. However, the $P_2S_6^{4-}$ units in $FePS_3$ were not destroyed during discharge-charge cycles. In terms of redox reactions, only iron was reduced during the first discharge cycle. In contrast, not only iron but also sulfur may be oxidized and reduced form the first charge cycle onward.

We further investigated the reaction mechanism of $FePS_3$ on the above results using density functional theory (DFT) calculations. The initial structural model was constructed with the assumption that the layered structure of $FePS_3$ with the $P_2S_6^{4-}$ unit does not significantly change during discharge-charge cycles according to the repeated appearance of the layered $FePS_3$ phase and undestroyed $P_2S_6^{4-}$ structural unit. It has been reported that transition-metal dichalcogenides, which have layer structures that are similar to that of $FePS_3$, have two different coordination geometries of $P_2S_6^{4-}$ units, namely trigonal prismatic and octahedral coordination geometries.[45,46] Hence, the coordination geometry of $P_2S_6^{4-}$ units in $FePS_3$ can change during the discharge-charge process. Four structure models of $FePS_3$ and $Li_{1.5}FePS_3$ with octahedral and trigonal prismatic symmetries were

constructed by Li^+ insertion between $FePS_3$ layers. Because the crystallinity of Li^+-inserted $FePS_3$ after discharge was low, these crystalline structural models were not consistent with the experimental structure. Nonetheless, some local structures would be represented in the model because these structural models are based on the experimental characterization and the local structural transition with octahedral and trigonal prismatic symmetries. Antimagnetic state within the layered structures were assumed.[47] The structure models that have been described were optimized using a first-principles calculation.

Figure 6 shows the optimized structures of (a) $FePS_3$ with octahedral $P_2S_6^{4-}$ units (octahedral $FePS_3$), (b) $Li_{1.5}FePS_3$ with octahedral $P_2S_6^{4-}$ units (octahedral $Li_{1.5}FePS_3$), (c) $FePS_3$ with trigonal $P_2S_6^{4-}$ units (trigonal $FePS_3$), and (d) $Li_{1.5}FePS_3$ with trigonal $P_2S_6^{4-}$ units (trigonal $Li_{1.5}FePS_3$). These optimizations showed some local structural change without changing the framework of octahedral $FePS_3$, octahedral $Li_{1.5}FePS_3$, and trigonal $FePS_3$. However, trigonal $Li_{1.5}FePS_3$ changes significantly owing to the structural optimization, and a rock salt-type structure that is attributable to bonds between sulfur and lithium was confirmed. As previously described, the experimental results showed the formation of a low-crystallinity phase which would be composed of various local structures. Thus, the local structures of the experimental low-crystallinity phase can be

represented by those of computationally calculated octahedral and/or trigonal $Li_{1.5}FePS_3$.

Table 1 shows the equilibrium voltage of the lithium intercalation reactions of $FePS_3$. At the first discharge cycle, the reaction corresponds to the formation of trigonal $Li_{1.5}FePS_3$ from octahedral $FePS_3$ (Table 1(B)) because the discharge plateau of around 0.9 V vs. Li-In at the first discharge cycle corresponded to the equilibrium voltage of the reaction between octahedral $FePS_3$ and trigonal $Li_{1.5}FePS_3$ (Table 1(B)). At the first charge cycle, no charge plateau was observed (Figure 1(a)). Hence, the reaction may correspond to two reactions between octahedral $FePS_3$ and trigonal $Li_{1.5}FePS_3$ (Table 1(B)) and between trigonal $FePS_3$ and trigonal $Li_{1.5}FePS_3$ (Table 1(D)). At the second discharge cycle, no discharge plateau was observed (Figure 1(b)). The discharge voltage at the second discharge cycle was higher than that at the first discharge cycle. Hence, the reaction of the second discharge cycle represents to two reactions between octahedral $FePS_3$ and trigonal $Li_{1.5}FePS_3$ (Table 1(B)), and between trigonal $FePS_3$ and trigonal $Li_{1.5}FePS_3$ (Table 1(D)). The calculated equilibrium voltages of these reactions at the first charge and the second discharge cycles were underestimated to the experimental charge and discharge voltages; there is small difference between charge and discharge voltages and OCV (Figure 1). A possible reason for the underestimated voltage is the difference between experimental $Li_{1.5}FePS_3$ and simplified models for DFT calculation. These

computational models are constructed assuming Li^+ insertion between $FePS_3$ layers and the coordination change between octahedral and trigonal coordination. However, the experimental XRD patterns showed low-crystalline phase(s), which was not completely represented by the computational structures. Thus, the redux reactions between $FePS_3$ and trigonal $Li_{1.5}FePS_3$ would be more complicated than computational ones.

Figure 7 presents density-of-states (DOSs) of (a) $FePS_3$ with octahedral $P_2S_6^{4-}$ units (octahedral $FePS_3$), (b) $Li_{1.5}FePS_3$ with octahedral $P_2S_6^{4-}$ units (octahedral $Li_{1.5}FePS_3$), (c) $FePS_3$ with trigonal $P_2S_6^{4-}$ units (trigonal $FePS_3$), and (d) $Li_{1.5}FePS_3$ with trigonal $P_2S_6^{4-}$ units (trigonal $Li_{1.5}FePS_3$). In octahedral and trigonal $FePS_3$, the states at the fermi level (E_f) were mainly composed of the states of iron (see Figure 7(a), (c)). In contrast, in octahedral and trigonal $Li_{1.5}FePS_3$, the states at E_f were composed of those of iron and sulfur (see Figure 7(b), (d)). Thus, the redox reaction of $FePS_3$ during discharge-charge cycles would be due to not only iron but also sulfur.

These simulation results indicate that only iron is reduced at the first discharge cycle, and that not only iron but also sulfur is oxidized and reduced from the first charge cycle onwards. The results of the redox of iron corresponded to the change in chemical states shown by the experimental results of Fe and S K-edge XANES spectra of the $FePS_3$ electrode.

4. Conclusion

The reaction mechanism of the $FePS_3$ electrode in all-solid-state lithium secondary batteries that use sulfide-based solid electrolytes was experimentally and computationally investigated. In the discharge-charge reaction ($FePS_3 + xLi^+ + xe^- \rightleftarrows Li_xFePS_3$, $0 \leq x \leq 1.5$), $P_2S_6^{4-}$ units were not destroyed during the first discharge cycle. However, the crystalline phase disappeared at the discharge cycle and $FePS_3$ appeared again at the charge cycle. In this discharge-charge reaction, the reversible reactions were confirmed by Fe and S K-edge X-ray absorption spectra. The reversible reactions were further investigated by the first-principle calculations, assuming the interlayered insertion of Li^+ with octahedral and trigonal coordination. The computational increase in the discharge voltage accompanied by the change in the chemical states of iron and sulfur supported the experimental results.

Acknowledgements

This work was partially supported by the Japan Science and Technology Agency (JST), Advanced Low Carbon Technology Research and development Program (ALCA), Specially Promoted Research for Innovative Next Generation Batteries

(SPRING) project, and Grant-in-Aid for JSPS Research Fellow (18J11169).

References

[1] J. M. Tarascon and M. Armand, *Nature*, **414**, 359 (2001).

[2] M. Armand and J. M. Tarascon, *Nature*, **451**, 652 (2008).

[3] K. Mizushima, P. C. Jones, P. J. Wiseman, and J. B. Goodenough, *Mater. Res. Bull.*, **15**, 783 (1980).

[4] J. Cho, Y. W. Kim, B. Kim, L. G. Lee, and B. Park, *Angew. Chem. Int. Ed.*, **42**, 1618 (2003).

[5] T. Ohzuku, A. Ueda, and M. Nagayama, *J. Electrochem. Soc.*, **140**, 1862 (1993).

[6] R. J. Gummow, A. de Kock, and M. M. Thackeray, *Solid State Ionics*, **69**, 59 (1994).

[7] O. Tsutomu and M. Yoshinari, *Chem. Lett.*, **2001**, 642.

[8] A. K. Padhi, N. S. Nanjundaswamy, and J. B. Goodenough, *J. Electrochem. Soc.*, **144**, 1188 (1997).

[9] A. R. Armstrong, M. Holzapfel, P. Novak, C. S. Johnson, S. H. Kang, M. M. Thackeray, and P. G. Bruce, *J. Am. Chem. Soc.*, **128**, 8694 (2006).

[10] M. M. Thackeray, S. H. Kang, C. S. Johnson, J. T. Vaughey, R. Benedeka, and S. A. Hackneyb, *J. Mater. Chem.*, **17**, 3112 (2007).

[11] N. Yabuuchi, K. Yoshii, S. T. Myung, I. Nakai, and S. Komaba, *J. Am. Chem. Soc.*, **133**, 4404 (2011).

[12] H. Yu and H. Zhou, *J. Phys. Chem. Lett.*, **4**, 1268 (2013).

[13] J. Zheng, P. Xu, M. Gu, J. Xiao, N. D. Browning, P. Yan, C. Wang, and J. G.

Zhang, *Chem. Mater.*, **27**, 1381 (2015).

[14] S. S. Zhang and D. T. Tran, *Electrochim. Acta*, **176**, 784 (2015).

[15] T. Matsuyama, M. Deguchi, K. Mitsuhara, T. Ohta, T. Mori, Y. Orikasa, Y. Uchimoto, Y. Kowada, A. Hayashi and M. Tatsumisago, *J. Power Sources*, **313**, 104 (2016).

[16] M. Tatsumisago, M. Nagao, and A. Hayashi, *J. Asian Ceram. Soc.*, **1**, 17 (2013).

[17] K. Takada, *Acta Mater.*, **61**, 759 (2013).

[18] F. Mizuno, A. Hayashi, K. Tadanaga, and M. Tatsumisago, *Adv. Mater.*, **17**, 918 (2005).

[19] N. Kamaya, K. Homma, Y. Yamakawa, M. Hirayama, R. Kanno, M. Yonemura, T. Kamiyama, Y. Kato, S. Hama, K. Kawamoto, and A. Matsui, *Nat. Mater.*, **10**, 682 (2011).

[20] S. Boulineau, M. Courty, J. M. Tarascon, and V. Viallet, *Solid State Ionics*, **221**, 1 (2012).

[21] Y. Kato, S. Hori, T. Saito. K. Suzuki, M. Hirayama, A. Mitsui, M. Yonemura, H. Iba, and R. Kanno, *Nat. Energy*, **1**, 16030 (2016).

[22] A. Hayashi, S. Hama, F. Mizuno, K. Tadanaga, T. Minami, and M. Tatsumisago, *Solid State Ionics*, **175**, 683 (2004).

[23] M. Tatsumisago, F. Mizuno, and A. Hayashi, *J. Power Sources*, **159**, 193 (2006).

[24] A. Sakuda, A. Hayashi, and M. Tatsumisago, *Chem. Mater.*, **22**, 949 (2010).

[25] M. Nagao, A. Hayashi, and M. Tatsumisago, *J. Mater. Chem.*, **22**, 10015 (2012).

[26] R. Koerver, I. Aygün, T. Leichtweiß, C. Dietrich, W. Zhang, J. O. Binder, P. Hartmann, W. G. Zeier, and J. Janek, *Chem. Mater.*, **29**, 5574 (2017).

[27] B. C. Kim, K. Takada, N. Ohta, Y. Seino, L. Zhang, H. Wada, and T. Sasaki, *Solid*

State Ionics, **176**, 2383 (2005).

[28] K. Takada, K. Iwamoto, and S. Kondo, *Solid State Ionics*, **117**, 273 (1999).

[29] U. Ulissi, S. Ito, S. M. Hosseini, A. Varzi, Y. Aihara, S. Passerini, *Adv. Energy Mater*, in press.

[30] J. E. Trevey, C. R. Stoldt, and S. E. Lee, *J. Electrochem. Soc.*, **158**, A1282 (2011).

[31] A. Hayashi, T. Matsuyama, A. Sakuda, and M. Tatsumisago, *Chem. Lett.*, **41**, 886 (2012).

[32] A. Sakuda, T. Takeuchi, K. Okamura, H. Kobayashi, H. Sakaebe, K. Tatsumi, and Z. Ogumi, *Sci. Rep.*, **4**, 4883 (2014).

[33] A. Sakuda, N. Taguchi, T. Takeuchi, H. Kobayashi, H. Sakaebe, K. Tatsumi, and Z. Ogumi, *Electrochem. Commun.*, **31**, 71 (2013).

[34] T. Matsuyama, A. Hayashi, T. Ozaki, S. Mori, and M. Tatsumisago, *J. Mater. Chem. A*, **3**, 14142 (2015).

[35] A. Sakuda, K. Ohara, K. Fukuda, K. Nakanishi, T. Kawaguchi, H. Arai, Y. Uchimoto, T. Ohta, E. Matsubara, Z. Ogumi, T. Okumura, H. Kobayashi, H. Kageyama, M. Shikano, H. Sakaebe, and T. Takeuchi, *J. Am. Chem. Soc.*, **139**, 8796 (2017).

[36] M. H. Lindic, H. Martinez, A. Benayad, B. Pecquenard, P. Vinatier, A. Levasseur, and D. Gonbeau, *Solid State Ionics*, **176**, 1529 (2005).

[37] A. Sakuda, A. Hayashi, and M. Tatsumisago, *Chem. Mater.*, **22**, 949 (2010).

[38] Y. Fujii, A. Miura, N. C. Rosero-Navarro, M. Higuchi, and K. Tadanaga, *Electrochim. Acta*, **241**, 370 (2017).

[39] K. Ichimura and M. Sano, *Synthetic Metals*, **45**, 203 (1991).

[40] Y. V. Kuzminskii, B. M. Voronin, and N. N. Redin, *J. Power Sources*, **55**, 133 (1995).

[41] A. Hayashi, H. Muramatsu, T. Ohtomo, S. Hama, and M. Tatsumisago, *J. Mater. Chem. A*, **1**, 6320 (2013).

[42] M. Scagliotti, M. Jouanne, M. Balkanski, G. Ouvrard, and G. Benedek, *Phys. Rev. B*, **35**, 7097 (1987).

[43] T. Takeuchi, H. Kageyama, K. Nakanishi, M. Tabuchi, H. Sakaebe, T. Ohta, H. Senoh, T. Sakai, and K. Tatsumi, *J. Electrochem. Soc.*, **157**, A1196 (2011).

[44] T. Hakari, M. Deguchi, K. Mitsuhara, T. Ohta, K. Saito, Y. Orikasa, Y. Uchimoto, Y. Kowada, A. Hayashi, and M. Tatsumisago, *Chem. Mater.*, **29**, 4768 (2017).

[45] W. B. Johnson and W. L. Worrell, *Synthetic Metals*, **4**, 225 (1982).

[46] M. Kertesz and R. Hoffmann, *J. Am. Chem. Soc.*, **106**, 3453 (1984).

[47] J. U. Lee, S. Lee, J. H. Ryoo, S. Kang, T. Y. Kim, P. Kim, C. H. Park, J. G. Park, and H. Cheong, *Nano Lett.*, **16**, 7433 (2016).

Table

Table 1 Calculated equilibrium voltage vs. Li-In for lithium intercalation reactions of $FePS_3$.

Reaction formula	Equilibrium voltage / V vs. Li-In*
(A) $FePS_3$ (O) + $1.5Li^+$ + $1.5e^-$ ⇄ $Li_{1.5}FePS_3$ (O)	0.62
(B) $FePS_3$ (O) + $1.5Li^+$ + $1.5e^-$ ⇄ $Li_{1.5}FePS_3$ (T)	0.88
(C) $FePS_3$ (T) + $1.5Li^+$ + $1.5e^-$ ⇄ $Li_{1.5}FePS_3$ (O)	1.02
(D) $FePS_3$ (T) + $1.5Li^+$ + $1.5e^-$ ⇄ $Li_{1.5}FePS_3$ (T)	1.27

$FePS_3$ (O): $FePS_3$ with octahedral $P_2S_6^{4-}$ units.

$FePS_3$ (T): $FePS_3$ with trigonal $P_2S_6^{4-}$ units.

$Li_{1.5}FePS_3$ (O): $Li_{1.5}FePS_3$ with octahedral $P_2S_6^{4-}$ units.

$Li_{1.5}FePS_3$ (T): $Li_{1.5}FePS_3$ with trigonal $P_2S_6^{4-}$ units.

*The calculated equilibrium voltage versus Li was converted to the equilibrium voltage versus Li-In using the potential of Li-In at 0.62 V vs. Li^+/Li.

Figure and captions

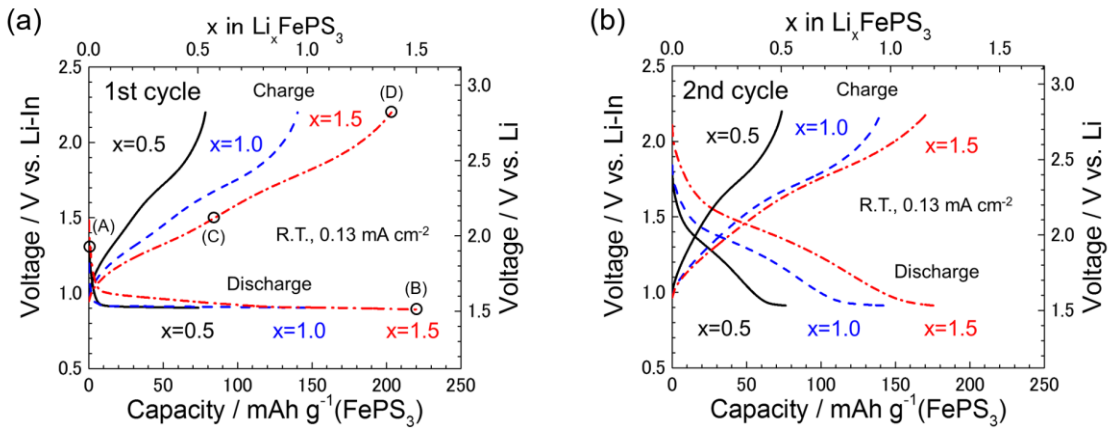


Figure 1. (a) First and (b) second discharge-charge curves of all-solid-state Li-In/75Li_2S·25P_2S_5 glass/$FePS_3$ batteries at 0.13 mA cm^{-2} at room temperature. In the first discharge cycle, 0.5 mol (black solid lines), 1.0 mol (blue dashed lines), and 1.5 mol (red dashed-dotted lines) of Li^+ was inserted per unit $FePS_3$. The open-circuit voltages (OCVs) were measured (A) before discharge and charge, (B) after first discharge, (C) at 1.5 V vs. Li-In during charge, and (D) after first charge.

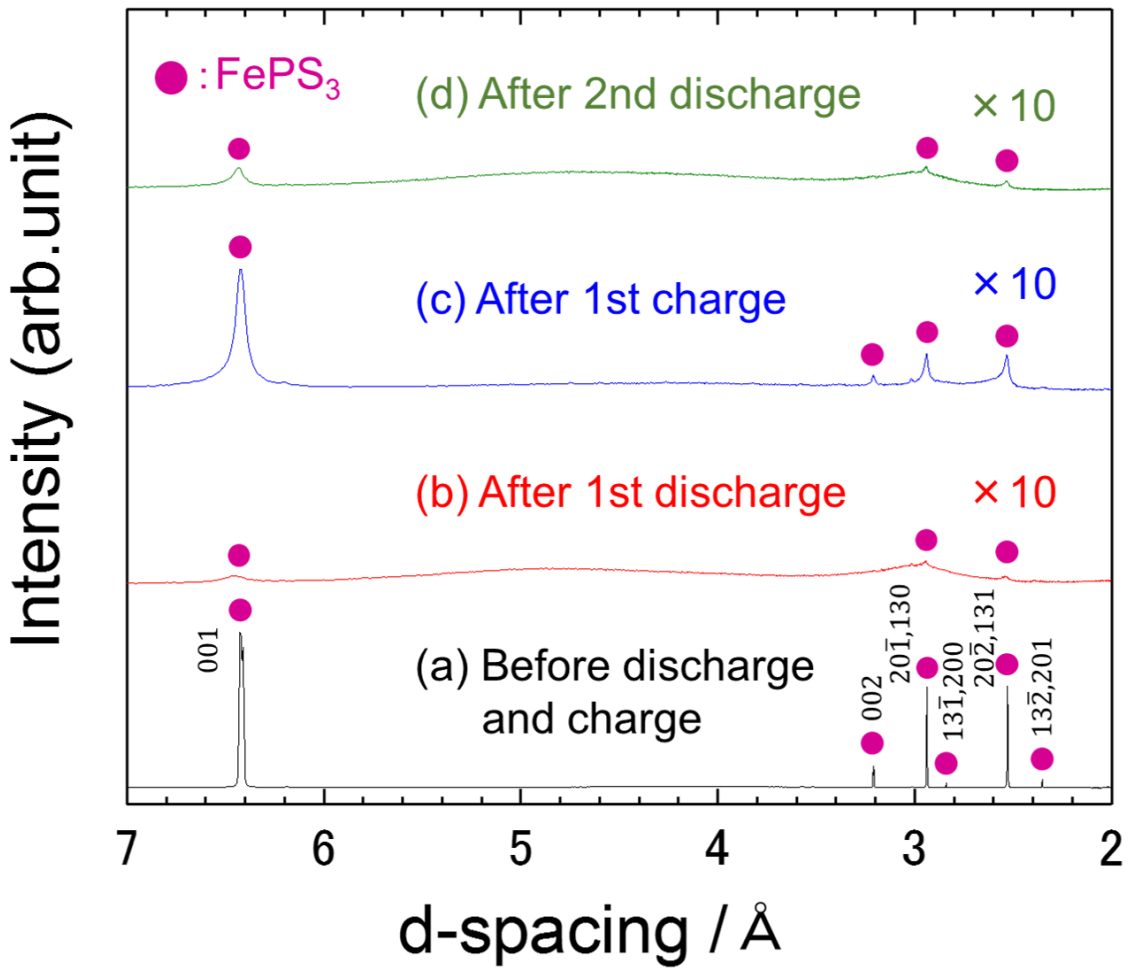


Figure 2. XRD patterns of the $FePS_3$ composite electrode (a) before discharge and charge, (b) after first discharge, (c) first charge, and (d) second discharge cycles. Solid circles denote peaks due to $FePS_3$.

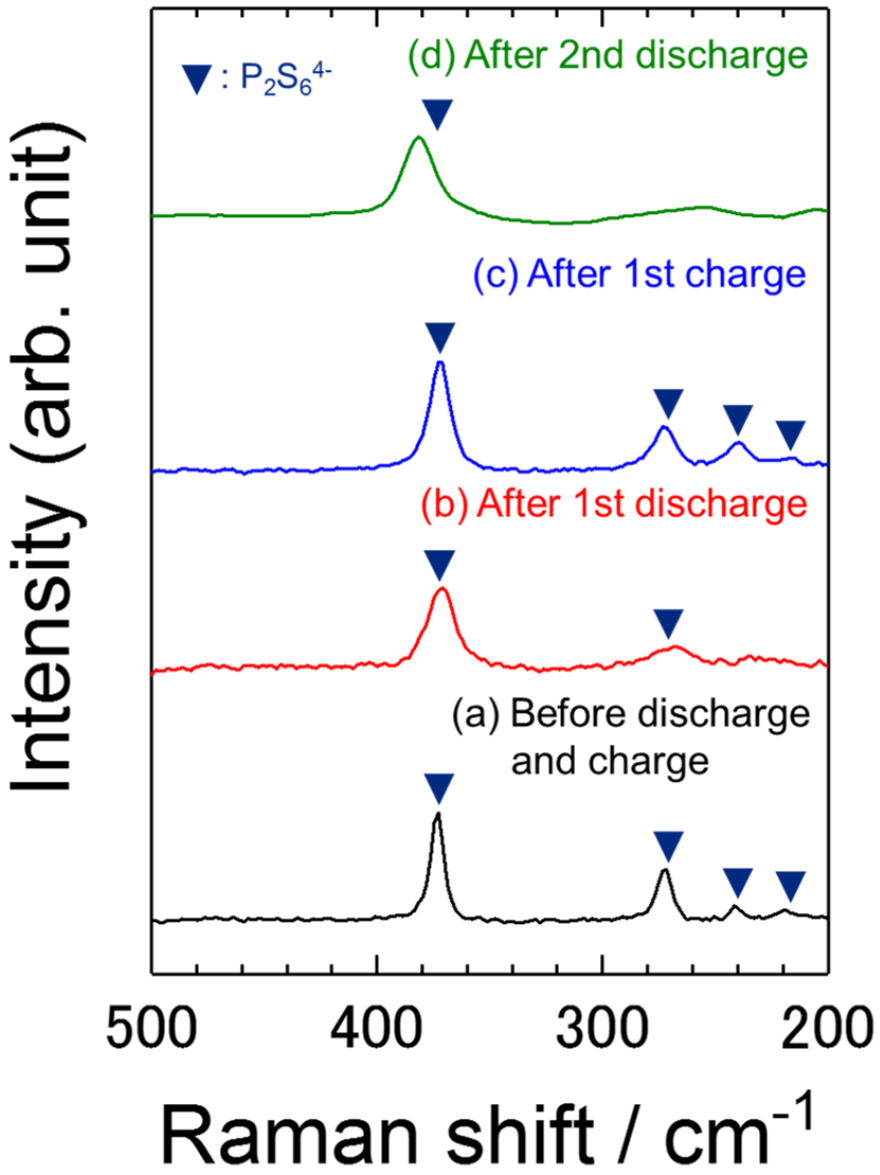


Figure 3. Raman spectra of the $FePS_3$ composite electrode (a) before discharge and charge, (b) after first discharge, (c) first charge, and (d) second discharge cycles. Solid inverted triangles denote Raman bands attributable to $P_2S_6^{4-}$.

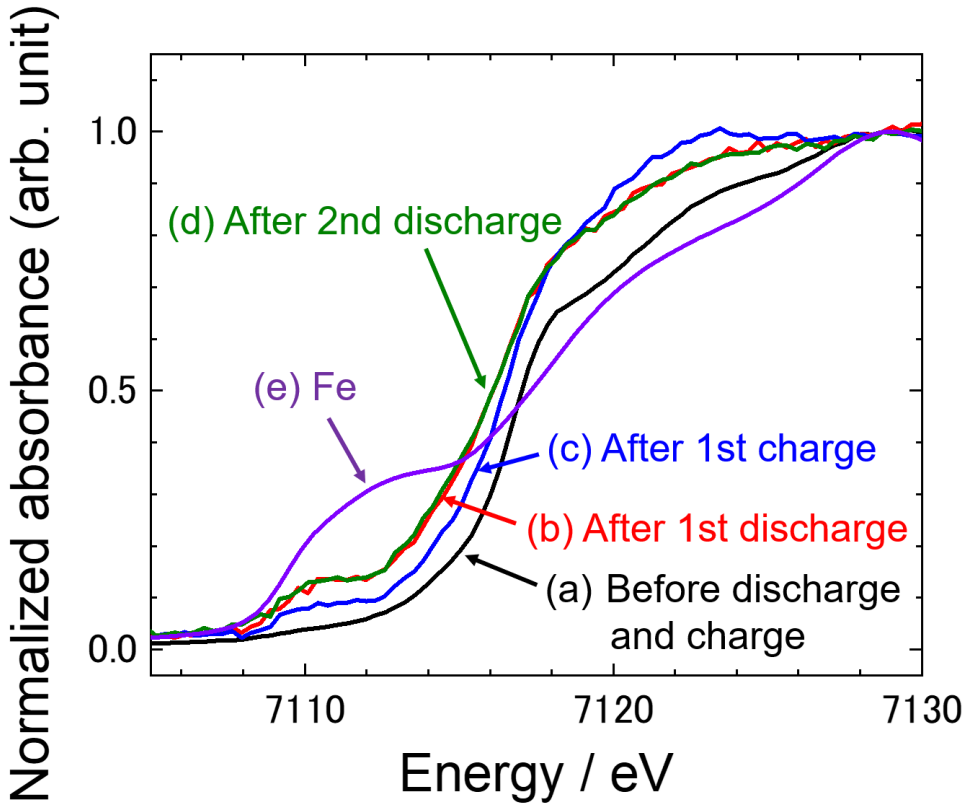


Figure 4. Fe K-edge XANES spectra of the $FePS_3$ composite electrode (a) before discharge and charge, (b) after first discharge, (c) first charge, and (d) second discharge cycles. For comparison, the spectrum of (e) Fe metal that is used as a reference is also shown.

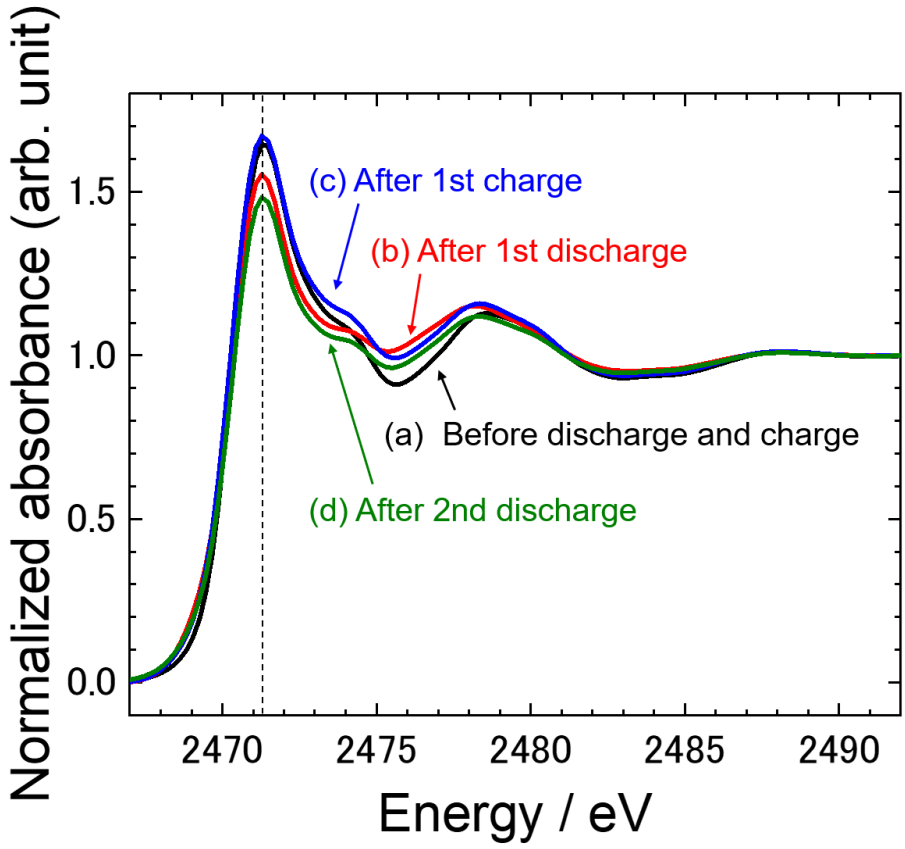


Figure 5. S K-edge XANES spectra of the $FePS_3$ electrode without solid electrolytes (a) before discharge and charge, (b) after first discharge, (c) first charge, and (d) second discharge cycles.

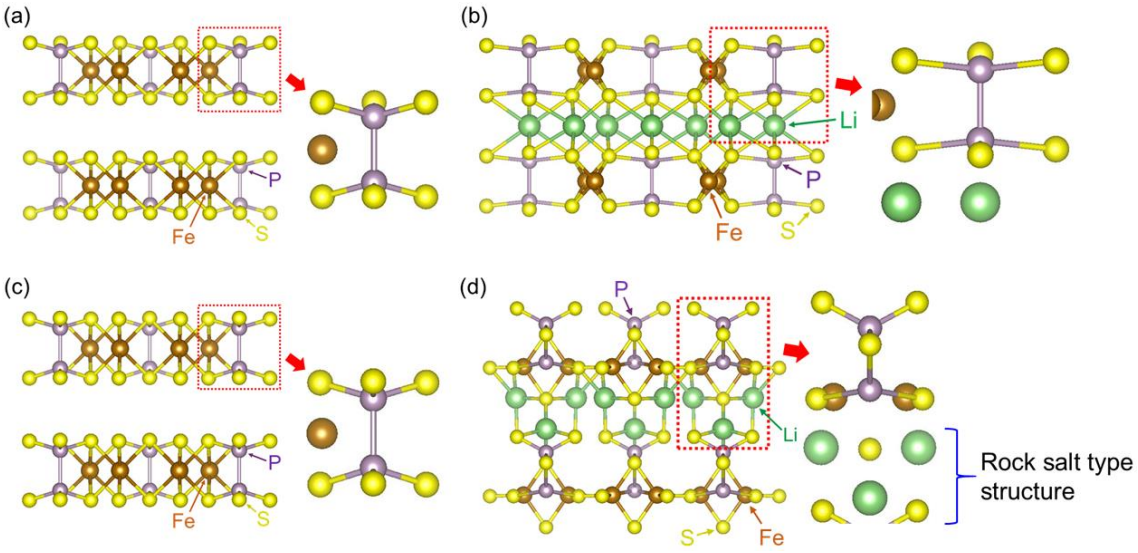


Figure 6. Optimized structures of (a) $FePS_3$ with octahedral $P_2S_6^{4-}$ units (octahedral $FePS_3$), (b) $Li_{1.5}FePS_3$ with octahedral $P_2S_6^{4-}$ units (octahedral $Li_{1.5}FePS_3$), (c) $FePS_3$ with trigonal $P_2S_6^{4-}$ units (trigonal $FePS_3$), and (d) $Li_{1.5}FePS_3$ with trigonal $P_2S_6^{4-}$ units (trigonal $Li_{1.5}FePS_3$).

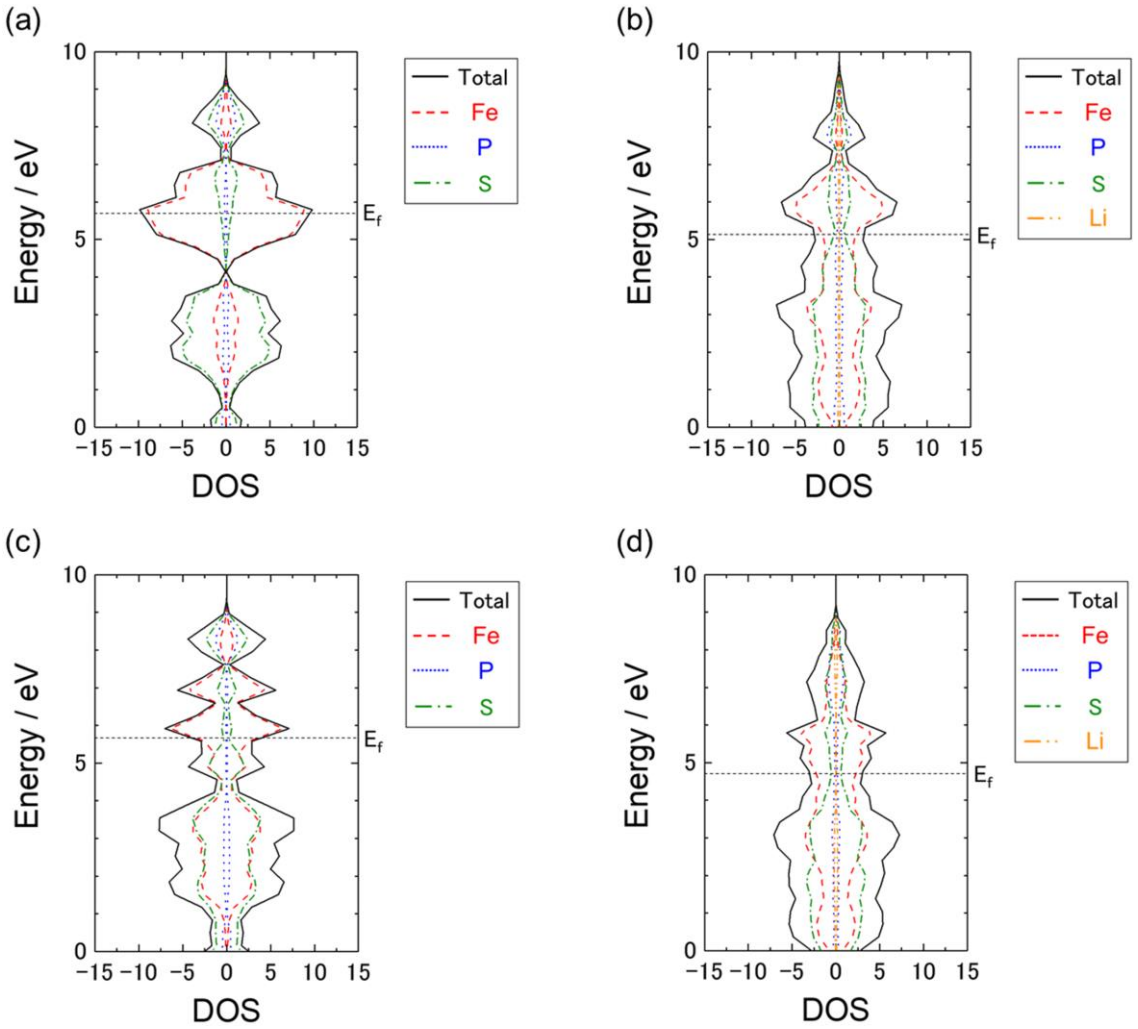


Figure 7. Density-of-states (DOSs) of (a) $FePS_3$ with octahedral $P_2S_6^{4-}$ units (octahedral $FePS_3$), (b) $Li_{1.5}FePS_3$ with octahedral $P_2S_6^{4-}$ units (octahedral $Li_{1.5}FePS_3$), (c) $FePS_3$ with trigonal $P_2S_6^{4-}$ units (trigonal $FePS_3$), and (d) $Li_{1.5}FePS_3$ with trigonal $P_2S_6^{4-}$ units (trigonal $Li_{1.5}FePS_3$).